α-Bungarotoxin Binding to Acetylcholine Receptor Membranes Studied by Low Angle X-Ray Diffraction

Howard S. Young, Leo G. Herbette,* and Victor Skita*
Department of Biochemistry, University of Alberta, Edmonton, Alberta, Canada T6G 2H7; and *Biomolecular Structure Analysis Center & Department of Biochemistry, University of Connecticut Health Center, Farmington, Connecticut 06030-2017

ABSTRACT The nicotinic acetylcholine receptor (nAChR) carries two binding sites for snake venom neurotoxins. α-Bungarotoxin from the Southeast Asian banded krait, *Bungarus multicinctus*, is a long neurotoxin which competitively blocks the nAChR at the acetylcholine binding sites in a relatively irreversible manner. Low angle x-ray diffraction was used to generate electron density profile structures at 14-Å resolution for *Torpedo californica* nAChR membranes in the absence and presence of α-bungarotoxin. Analysis of the lamellar diffraction data indicated a 452-Å lattice spacing between stacked nAChR membrane pairs. In the presence of α-bungarotoxin, the quality of the diffraction data and the lamellar lattice spacing were unchanged. In the plane of the membrane, the nAChRs packed together with a nearest neighbor distance of 80 Å, and this distance increased to 85 Å in the presence of toxin. Electron density profile structures were calculated in the absence and presence of α-bungarotoxin, revealing a location for the toxin binding sites. In native, fully-hydrated nAChR membranes, α-bungarotoxin binds to the nAChR outer vestibule and contacts the surface of the membrane bilayer.

INTRODUCTION

The nicotinic acetylcholine receptor (nAChR) is a ligand-gated ion channel (LGIC) found in the neuromuscular junction of vertebrates and the electrocytes of electric fish. The nAChR in the electrocyte membranes of the electric marine ray, *Torpedo*, is the best characterized member of a superfamily of LGICs involved in information transfer in the brain and neuromusculature. The nAChR is a large complex of four transmembrane glycoprotein subunits which form an $\alpha_2\beta\gamma\delta$ pentameric complex surrounding a central cation-conducting pore (Raftery et al., 1980). The subunits form 120-Å rods arranged around a pseudo-fivefold axis and lying approximately normal to the membrane plane (Toyoshima and Unwin, 1988, 1990; Unwin, 1993, 1995; Miyazawa et al., 1999).

The nAChR carries two binding sites for agonists and competitive antagonists and a single binding site for non-competitive blockers. Acetylcholine is the natural agonist at nicotinic synapses, and the two α-subunits per receptor complex contain the agonist binding sites. Polypeptide neurotoxins act as competitive antagonists and include the venoms from snakes of the Elapidae (cobras, kraits, mambas, coral snakes, etc.) and Hydrophidae (sea snakes) families. These venoms contain basic polypeptides which are grouped into short- and long-chain neurotoxins (Chiapinelli, 1993). α-Bungarotoxin (α-toxin) from the Southeast Asian banded krait, *Bungarus multicinctus*, is a long neurotoxin with high affinity for nAChRs (Lukas et al., 1981; Servent et al., 1997).

Our understanding of α-toxin binding has progressed rapidly with the recent crystal structure of the acetylcholine binding protein (AChBP) (Brejc et al., 2001) and numerous α-toxin structures by x-ray crystallography (Agard and Stroud, 1982; Love and Stroud, 1986; Betzel et al., 1991; Harel et al., 2001) and NMR (Leroy et al., 1994; Zinn-Justin et al., 1992; Moise et al., 2002). The AChBP is a homolog of the extracellular domain of nAChR and the crystal structure has allowed interpretation of the electron cryomicroscopy structure of nAChR (Unwin et al., 2002). α-Toxin has been shown to bind to the α-subunit between residues 172-205 (Wilson et al., 1985; Wilson and Lentz, 1988; Mulac-Jericevic and Atassi, 1986; Neumann et al., 1986a,b; Ralston et al., 1987). Moreover, the structures of α-toxin in complex with some of these α-subunit sequences have been determined (Basus et al., 1993; Harel et al., 2001; Zeng et al., 2001; Scherf et al., 1997; Moise et al., 2002). These data combined with the AChBP crystal structure form the basis for current models of α-toxin binding (Harel et al., 2001; Moise et al., 2002).

The goal of this study was to provide direct evidence for the location of the α-toxin binding sites on native nAChR membranes. Utilizing the technique of low angle x-ray diffraction, relative electron density profiles were calculated for fully oriented *Torpedo* nAChR membranes in the absence and presence of α-toxin. Comparison of the relative electron density profiles in the absence and presence of α-toxin indicated a location for the binding sites in contact with the membrane surface. Our data, combined with the current understanding of nAChR structure, provide a structural model for α-toxin binding.

MATERIALS AND METHODS

Membrane preparation

nAChR-enriched membrane fragments were prepared from *T. californica* (Klymkowsky et al., 1980; Kistler and Stroud, 1981). Fifty grams of frozen

Submitted February 17, 2003, and accepted for publication April 21, 2003.

Address reprint requests to Dr. Howard S. Young, Tel.: 780-492-3931; E-mail: hyoung@biochem.ualberta.ca.

Leo G. Herbette's present address is Exploria, 151 New Park Ave., Suite 15, Hartford, CT 06106.

Victor Skita's present address is Indus International, Inc., 60 Spear St., San Francisco, CA 94105.

0006-3495/03/08/943/11 $2.00

electric organ (Marinus Inc., Long Beach, CA; stored at −70°C) were homogenized in 300 ml of homogenization buffer (10 mM NaH_2PO_4, pH 7.4, 400 mM NaCl, 5 mM EDTA, 5 mM EGTA, 5 mM iodoacetamide, 5 mM NEM, 0.4 mM PMSF in 2-propanol, 0.3 mM DFP, 0.02% NaN_3) in a VirTis homogenizer (model 45, VirTis Co., Gardner, NY). The crude homogenate was centrifuged for 10 min at 6500 rpm in an SW-28 rotor (Beckman Instruments, Inc., Palo Alto, CA). The resulting supernatant was collected through 16 layers of cheesecloth and centrifuged for 55 min at 19,500 rpm (~50,000 × *g*). The pelleted membranes were resuspended in 50 ml gradient buffer (10 mM NaH_2PO_4, pH 7.8, 1 mM EDTA, 1 mM EGTA, 2.5 mM iodoacetamide, 0.2 mM PMSF, 0.3 mM DFP, 0.02% NaN_3) by homogenization in a 50-ml Dounce homogenizer. After two rounds of centrifugation for 10 min at 6500 rpm to remove precipitate, the membranes were pelleted for 55 min at 19,500 rpm. The pelleted membranes were resuspended in 5 ml 20% wt/wt sucrose and layered onto a single 35-ml, 38% to 29% (weight/weight) linear sucrose gradient in gradient buffer. The gradient was centrifuged overnight (≥12 h) at 25,000 rpm in an SW-28 rotor and fractionated from the bottom into 1-ml fractions.

The sucrose gradient fractions were analyzed by SDS-PAGE (Laemmli, 1970). ^{125}I-α-Bungarotoxin (Amersham Corp., Arlington Heights, IL) binding was measured by a filter binding assay (Schmidt and Raftery, 1973). Negative-stain electron microscopy was carried out using either 2% sodium phosphotungstate, pH 7.4, or 1% uranyl acetate, pH 6.0.

Diffraction sample preparation

Fully oriented nAChR membrane multilayer samples were prepared by extended centrifugation followed by partial dehydration. A total of 300 μg membrane protein in gradient buffer, pH 7.4, were placed in a Delrin sedimentation cell (Chester et al., 1987) containing an ultrathin aluminum foil (0.008-mm thickness; Goodfellow Corp., Berwyn, PA) or PET substrate (0.023-mm thickness; Goodfellow). The membrane suspension and cell were centrifuged at 28,000 rpm (~110,000 × *g*) for 24 h in an SW-28 rotor. Immediately after centrifugation, the supernatant was aspirated from the membrane pellet, and the pellet on the substrate was removed and mounted on a curved glass support. The sample was partially dehydrated to 100%, 98%, or 96% relative humidity (H_2O, saturated K_2SO_4, or saturated KNO_3, respectively) for a period of 24 h in a sealed brass canister. Sample temperature was maintained at 4°C.

Low angle x-ray diffraction

Cu K x rays produced by an Elliot GX-18 rotating anode x-ray generator (Enraf Nonius Co., Bohemia, NY) were point focused with orthogonal Frank's mirror assemblies. Monochromatic Cu K_α x rays ($\lambda = 1.54$ Å) were selected by filtering with Ni foils. Slit collimation and helium filled beam paths were used to reduce background scatter. Diffraction data were recorded on DEF-5 film (Eastman Kodak Co., Rochester, NY) and typically involved a stack of 5 films and a 48-h exposure at a sample-to-detector distance of ~21 cm. Sample temperature was maintained at 4°C.

Additional diffraction data at sample-to-detector distances from 60 cm to 2 m were collected at beamline X9-A, Brookhaven National Laboratories, National Synchrotron Light Source, Upton, NY (Pachence et al., 1989). Monochromatic x rays of $\lambda = 1.54$ Å were used; sample temperature was maintained at 4°C.

Data analysis and reduction

Film data were digitized on an Optronics P-1700 rotating drum scanner (Optronics International Inc., Chelmsford, MA) using a 25-μm aperture size. Digitized images were integrated using a radial-butterfly integration routine which accounted for incident x-ray beam height and sample mosaic spread (Gruner et al., 1982). First, a linear background was subtracted from the data as a function of the number of pixels included in the radial integration. Second, ''parasitic'' scatter by the x-ray optics and sample mount was experimentally measured and matched to the sample data in the final stage of the data reduction procedure. All five films in the lamellar diffraction data collection were digitized, integrated and reduced as described. To obtain the intensity function from the reduced film data, films were scaled to one another by the appropriate power of the film factor, *f*. An average film factor of 3.2 ± 0.5 ($n = 21$) (Phillips and Phillips, 1985) yielded satisfactory overlap of the diffraction maxima on the films in the stack. The raw intensity data were converted to units of s ($s = 2\sin(\theta)/\lambda$), where 2θ is the angle between the incident and scattered beam for a particular reflection. The resultant intensity function was Lorentz corrected by $s = 2\sin(\theta)/\lambda$ to obtain the experimental intensity function, $I_{exp}(s)$. Finally, for each experimental data set, the total corrected and integrated intensity was scaled to a constant value in order to compare data sets between samples (Moody, 1963; Blaurock, 1971).

The structure factor amplitudes, $|F_{exp}(s)|$, calculated as the square root of $I_{exp}(s)$, were determined by fitting with a series of Gaussian functions. The Gaussian functions were constrained to have mean values coinciding exactly with reciprocal lattice positions and full-width-at-half-maximum (FWHM) consistent with the amount of lattice disorder in the diffraction samples. In fitting the lamellar diffraction data with a series of Gaussians, the FWHM were determined experimentally for reflections $l = 3$, 4, and 5. This was done using synchrotron radiation and a sample-to-detector distance of 2 m. The Gaussian fits for the remaining reflections were extrapolated linearly from these experimentally determined FWHM. This resulted in the Gaussian width increasing with s. This procedure yielded $|F_{Gfit}(s)|$, $|F_{exp}(s)|$ described as a sum of Gaussian functions. Residuals were calculated as

$$R = \Sigma[|F_{exp}(s) - F_{Gfit}(s)|/|F_{exp}(s)|] \quad (1)$$

to judge the extent of agreement between the experimental and the fitted structure factor amplitudes.

The structure factor amplitudes were phased by a pattern recognition approach (Luzzati et al., 1972) in which every unique phase combination was calculated and the resultant electron density profiles were judged based on known or postulated properties of the membrane system. Several criteria were then applied in judging a correct phase set: 1), the presence of two lipid bilayer structures in the double membrane unit cell providing the highest contrast elements in our diffraction experiments (Franks and Levine, 1981); 2), our current structural understanding of this membrane system (Toyoshima and Unwin, 1988, 1990; Unwin, 1993, 1995; Miyazawa et al., 1999); and 3), the presence or absence of nonzero intensity levels between reflections indicating a likely phase change. These phasing methods were then assessed for their agreement and a unique phase set was assigned (for further details, see Results).

The structure factor amplitudes and phases were used to calculate a relative electron density profile, $\rho_{exp}(z)$, for the nAChR membrane multilayers. As an alternative to Gaussian fitting, the $I_{exp}(s)$ was treated as a continuous Fourier transform. The continuous $|F_{exp}(s)|$ function and the phases were used to calculate a relative electron density profile, $\rho_{exp}(z)$, for the nAChR membrane multilayers.

Error in $I_{exp}(s)$ and $\rho_{exp}(z)$ was calculated as a point-by-point standard deviation of the population, and was displayed as an envelope of uncertainty around a mean for $I_{exp}(s)$ and $\rho_{exp}(z)$.

Model calculation

Modeling of the interaction between the nAChR and α-toxin was undertaken (Chester et al., 1992). For a careful analysis of the expected difference electron density profiles, the AChBP (1I9B; Brejc et al., 2001) and α-toxin (1KL8; Moise et al., 2002) were used in model calculations. A complex of AChBP and two α-toxin molecules was constructed (Moise et al., 2002) and the number of electrons was projected onto the z axis parallel with the AChBP channel (Chester et al., 1992). The projected electron density profiles are atomic resolution models of the nAChR synaptic domain in the absence and presence of two α-toxin molecules.

RESULTS

Membrane preparation

The purified nAChR membrane vesicles were evaluated by quantitative SDS-PAGE and ^{125}I-α-bungarotoxin binding (data not shown). A representative polyacrylamide gel and the four peak fractions typical of those used in the diffraction studies are shown in Fig. 1. The sucrose gradient peak fractions were ~85% nAChR by weight protein, including rapsyn which is normally associated in a 1:1 stoichiometry with the receptor (LaRochelle and Froehner, 1986). Furthermore, negative-stain electron microscopy revealed a homogeneous preparation with >95% of the membrane vesicles between 0.5 μm and 1.5 μm in diameter and densely packed with nAChRs (data not shown).

Low angle x-ray diffraction

The equatorial and lamellar diffraction data from nAChR membrane samples are shown in Fig. 2. The equatorial diffraction data (Fig. 2 *a*) revealed hexagonal packing of the nAChR molecules in the plane of the membrane with a center-to-center distance of 80 Å ± 1 Å ($n = 17$) in the absence of α-toxin, and this distance increased to 85 Å ± 1 Å ($n = 6$) in the presence of α-toxin. Predominantly oriented on the equatorial axis were observed broad bands of continuous diffraction centered at 10 Å and 4.6 Å. Diffraction at 4.6 Å was characteristic of nonspecific liquid crystalline chain packing of the lipid molecules in a bilayer organization. Diffraction near 10 Å with a degree of orientation in the plane of the membrane has been reported for the purple membrane (Blaurock, 1975), visual-cell disc membranes (Blaurock and Wilkins, 1969), red blood cells (Lesslauer, 1978), sarcoplasmic reticulum membranes (Herbette et al., 1977), and gap junction membranes (Makowski et al., 1977). Invariably, this diffraction has been interpreted as α-helical secondary structure with an average orientation perpendicular to the plane of the membrane.

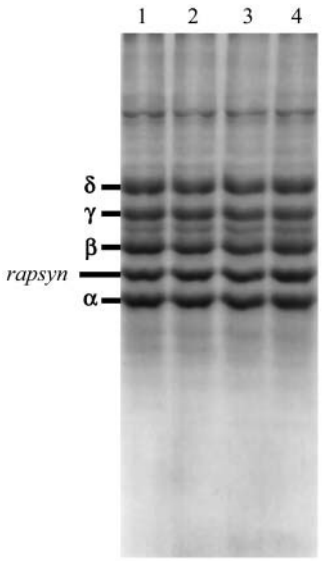

FIGURE 1 SDS-PAGE (0.1% SDS/10% polyacrylamide gel) of the four peak fractions from a linear sucrose density gradient. These peak fractions occurred at 36% to 37% sucrose and were ~85% nAChR by weight protein (including rapsyn). The gel shown is representative of the nAChR membrane preparations used in the diffraction studies. The α, β, γ, and δ subunits and rapsyn are indicated in the figure.

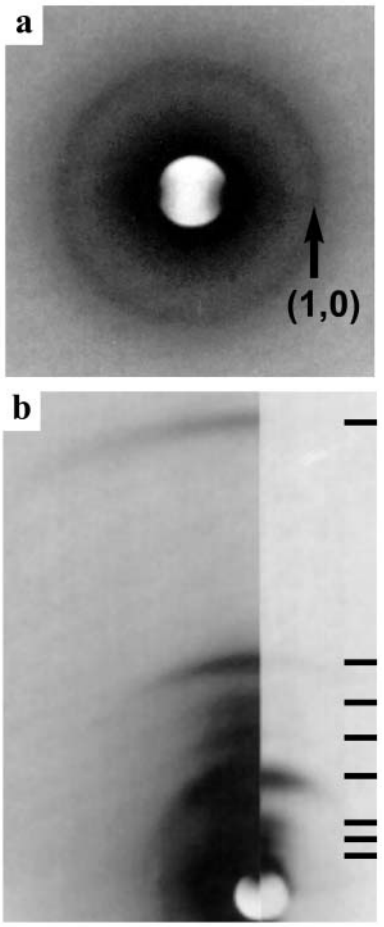

FIGURE 2 Representative low angle x-ray diffraction patterns obtained from fully oriented nAChR membranes at 96% relative humidity, a sample-to-detector distance of 21 cm, and a 48-h exposure for a 5-film stack. (*a*) Equatorial diffraction data collected in transmission geometry at a sample-to-detector distance of 21 cm. The beamstop shadow is in the center of the film. The (1,0) reflection is readily apparent in the figure as a ring at low angle ($s = 1/69.3$ Å^{-1}) as indicated by the *arrow*, while the (1,1) and (2,0) were diffuse rings at higher angle (not shown). These reflections indexed on a hexagonal lattice with an average center-to-center spacing of 80 Å ± 1 Å ($n = 17$). (*b*) Lamellar diffraction data, with the lamellar axis oriented vertically and the equatorial axis oriented horizontally. The beamstop shadow is at the intersection of these two axes. The left half of the figure is the first film in the stack and the right half of the figure is the fourth film. The lamellar lattice spacing for this sample was 454 Å ± 3 Å with the diffraction maxima indexed as (0,0,*l*) for $l = 3$, $l = 4$, $l = 5$, $l = 8$ ($s = 1/57$ Å^{-1}), $l = 11$, $l = 13$, $l = 16$ ($s = 1/28$ Å^{-1}), and $l = 32$ ($s = 1/14$ Å^{-1}). The lamellar lattice positions are indicated on the right-hand side from bottom to top for $l = 3$, $l = 4$, $l = 5$, $l = 8$, $l = 11$, $l = 13$, $l = 16$, and $l = 32$.

Fig. 2 *b* is representative of the lamellar diffraction data obtained from nAChR membranes. The lamellar lattice spacing for this sample was 454 Å ± 3 Å with a maximum resolution of 14 Å recorded on this film. The lamellar diffraction from these samples extended to ~8 Å resolution on average. Despite the moderate resolution x-ray diffraction exhibited by these samples, sample disorder was a complicating factor in our interpretation. Disorder of the first kind, or mosaic spread, is due to microdomains or crystallites in the sample (Hosemann and Bagchi, 1962). Mosaic spread can be quite severe, yet high resolution diffraction can still be observed (e.g., a salt powder pattern). Disorder of the second kind, or lattice disorder, reflects the number of ordered membranes within a crystallite (Hosemann and Bagchi, 1962; Schwartz et al., 1975; Blaurock, 1982) and is a primary determinant of resolution. For our nAChR membrane multilayers, Patterson analysis (Chester et al., 1992; Young et al., 1992) revealed an average of three ordered membranes per crystallite (data not shown) with a mosaic spread of 30–40° (Fig. 2 *b*). Even with the apparent lattice disorder, lamellar diffraction was readily observed beyond 14 Å with a maximum Bragg-order of $l = 32$ used in these studies ($d/32 = 14$ Å, where $d = 452$ Å). This is not unexpected because reflections $l = 8$, 16, and 32 arise primarily from the membrane lipid bilayer (Chester et al., 1992).

The digitized, integrated, background-corrected, and Lorentz-corrected $I_{exp}(s)$ is shown in Fig. 3 *a*. The intensity function is the composite of data collected on rotating-anode and synchrotron x-ray sources. The average lattice spacing for the nAChR membrane multilayers was 452 Å ± 5 Å ($n = 21$). A linear regression analysis of the integer lattice position, l, versus the center-of-mass position for each reflection in reciprocal Angstroms gave a slope of 452 Å (σ_{slope} was 3 Å with a correlation of 0.99990). The maximum deviation of the center-of-mass position for any reflection from the true lattice position was less than 1% and was randomly distributed.

The next stage in the data analysis involved determination of the structure factor amplitudes from $I_{exp}(s)$. The structure factor modulus, $|F_{exp}(s)|$, calculated as the square root of $I_{exp}(s)$, was fitted with a series of Gaussian functions taking into account the apparent lattice disorder. The Gaussians were constrained to have mean values exactly at reciprocal lattice positions (l/d, where l is an integer and $d = 452$ Å) and FWHM consistent with the amount of lattice disorder in the sample. Using synchrotron radiation and long sample-to-detector distances, the FWHM for reflections $l = 3$, 4, and 5 were determined experimentally. The Gaussian fits for the remaining reflections were extrapolated linearly from these experimentally determined FWHM. This resulted in the Gaussian widths increasing with s. A representative result is shown in Fig. 3 *b* with the $|F_{exp}(s)|$ and the individual Gaussians used in the fit. Residuals were calculated to judge the agreement between $|F_{exp}(s)|$ and $|F_{Gfit}(s)|$ and were determined to have a mean value of $R_{mean} = 0.13$ ($n = 21$).

Two basic approaches were used to determine a set of phases. For a centrosymmetric unit cell the only possible phase choices are zero or π radians. Therefore, for the observed lamellar diffraction there were 2^8 (256) possible phase combinations, which reduced to 64 phase combinations after eliminating simple profile inversions and shifts in the unit cell origin. The first phasing method used a pattern recognition approach (Luzzati et al., 1972). The 64 unique phase combinations were used to generate electron density profile structures, and these 64 electron density profiles were visually inspected for the presence of two apposed lipid bilayer structures in the double-membrane unit cell. Surprisingly, only 2 out of the 64 phase combinations possessed clearly defined lipid bilayer structures (Wiener and White, 1992). The remaining two profile structures were compared against known structural information on the nAChR and found to be in general agreement (in terms of the protein mass distribution across the membrane). The second phasing approach utilized synchrotron radiation and long sample-to-

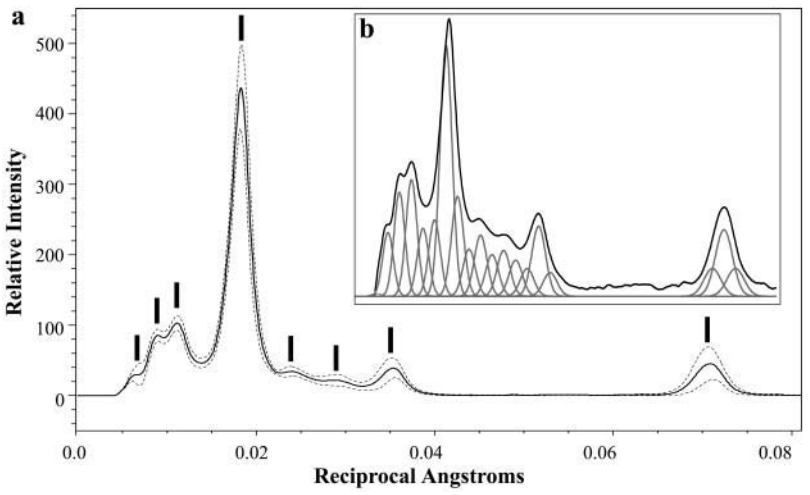

FIGURE 3 (*a*) $I_{exp}(s)$ derived from the digitized, integrated and corrected film data. The intensity data is plotted as relative intensity (arbitrary units) versus reciprocal Angstroms (in units of s, where $s = 2\sin(\theta)/\lambda$). The solid line is the average of 21 samples from 10 membrane preparations, and is surrounded by an envelope of uncertainty calculated as a point-by-point standard deviation of the population (*dashed lines*). As in Fig. 2, the lamellar lattice positions are indicated from left to right for $l = 3$, $l = 4$, $l = 5$, $l = 8$, $l = 11$, $l = 13$, $l = 16$, and $l = 32$. The center-of-mass position of each diffraction maxima in reciprocal Angstroms was plotted versus integer lattice position, l. The slope of a linear regression fit was 452 Å with a σ_{slope} of 3 Å and a correlation of 0.99990. (*b*) An example of the Gaussian fitting of $|F_{exp}(s)|$. $|F_{exp}(s)|$ is shown as a black line and was calculated as the square root of $I_{exp}(s)$, and the Gaussians used in the fit are shown as gray lines. The final fit between $|F_{exp}(s)|$ and $|F_{Gfit}(s)|$ yielded a mean residual of $R = 0.13$ ($n = 21$).

detector distances to discern discontinuities in the lamellar diffraction data. A sharp discontinuity, or zero intensity level, observed between the $l = 3$ and $l = 4$ reflections indicated a possible phase change.

Of the 256 possible phase combinations, only a single phase set was consistent with both the known structure of the nAChR membrane and the positions of zero and nonzero intensity levels between lamellar reflections (Table 1). Two phase sets satisfied our first selection criteria and gave a double-membrane unit cell with two apposed lipid bilayer structures. These two phase sets were reduced to a single, unique phase set based on the sharp discontinuities in intensity level detected between $l = 3$ and $l = 4$ (possible phase change), between $l = 5$ and $l = 8$ (phase change), and between $l = 8$ and $l = 11$ (phase change). Conversely, nonzero intensity levels between reflections indicated no phase change, as observed between $l = 4$ and $l = 5$. Thus, the final phase set was the most likely phase combination consistent with both the experimental information presented in this study and our current structural understanding of this membrane system. Moreover, this phase set was determined to be the only acceptable phase combination based on low angle x-ray diffraction studies of *Torpedo* nAChR membranes in the presence of α-toxin (discussed below).

TABLE 1 Summary of the structure factor amplitudes and phases for the nAChR membranes in the absence and presence of α-bungarotoxin

Miller indices (0,0,*l*)	Integrated intensity*		Phase†	
	− Toxin	+ Toxin	− Toxin	+ Toxin
1	N/A‡	N/A		
2	N/D§	N/D		
3	27152	57088	0 or π	π
4	70134	146329	0	0
5	95307	183849	0	0
6	0	0		
7	16700	55778	π	π
8	705525	675346	π	π
9	110865	110865	π	π
10	0	0		
11	42476	52928	0	0
12	20005	22859	0	0
13	19299	19299	0	0
14	0	0		
15	5921	4447	π	π
16	37221	41353	π	π
17	6317	1797	π	π
31	653	653	π	π
32	84881	77504	π	π
33	688	688	π	π

*Integrated intensities are the structure factors amplitudes determined by Gaussian fitting as described in Materials and Methods.

†Phases were determined by the pattern recognition approach of Luzzati et al. (1972). A sharp minimum in intensity level between $l = 3$ and $l = 4$ suggested that these two reflections have opposite phases. This was later confirmed by the pattern recognition approach in the presence of α-bungarotoxin.

‡Not apparent. The first Bragg order must be nearly zero. Grazing-incidence small angle x-ray scattering was performed using synchrotron radiation and a sample-to-detector distance of 2 m. A first Bragg order was never found.

§Not determined. A weak second Bragg order was observed, but its intensity could not be accurately determined. The effect of a weak second order on the nAChR profile structure was negligible.

Fig. 4 is the 14-Å resolution electron density profile structure for the nAChR membrane calculated from the structure factor amplitudes and phases described above. For the profile structure of Fig. 4, *a* and *b*, the structure factor amplitudes were determined by Gaussian decomposition as described above. As an alternative to Gaussian decomposition, the intensity function was treated as a continuous Fourier transform and the electron density profile was calculated by applying the phases to the continuous $|F_{exp}(s)|$ function (Fig. 4 *c*). Comparison of these two electron density profiles, calculated using very different methods, revealed significant differences only at the edges of the unit cell. One can infer from this that small changes in the Gaussian FWHM used for decomposition would result in negligible changes in the electron density profile. Moreover, the method of interpretation had no effect on the difference electron density profile calculated in the presence of α-toxin.

Clearly visible in the nAChR double-membrane unit cell (Fig. 4 *a*) are slightly asymmetric lipid bilayer structures with the methyl-troughs centered at ±56.5 Å and phospholipid headgroup-to-headgroup spacings of 43 Å (Ross et al., 1977). The two apposed nAChR membranes are oriented with their cytoplasmic domains toward the *x* axis origin. One-half of the double membrane unit cell is shown for clarity in Fig. 4 *b*, and our interpretation of the profile structure is shown in Fig. 4 *c*. The nAChR cytoplasmic domain and rapsyn extended 35 Å from the bilayer surface. The synaptic domain of the nAChR appeared to extend as far as 90 Å above the bilayer surface followed by another extensive region at the edge of the unit cell (±197 Å). This region at the edge of the unit cell was attributed to the ~20 kDa of glycosylation attached to the nAChR (Nomoto et al., 1986; Poulter et al., 1989) which would remain highly hydrated in these experiments. Excluding glycosylation, our results gave a total molecular length for the nAChR (including rapsyn) of 168 Å, consistent with mean radial density distributions from tubular crystals of nAChR membranes (Toyoshima and Unwin, 1988, 1990).

Low angle x-ray diffraction in the presence of α-toxin

To evaluate differences in the electron density profile in the absence and presence of α-toxin, six sets of matched samples from three separate membrane preparations were prepared. Fig. 5 summarizes the low angle x-ray diffraction data from these six sets of matched samples. At this point, it is necessary to consider some aspects of the error in determining $I_{exp}(s)$. The envelope of uncertainty in $I_{exp}(s)$ translated into an error of ~22% [$|\Delta I(s)|/I(s)$]. However, this error included

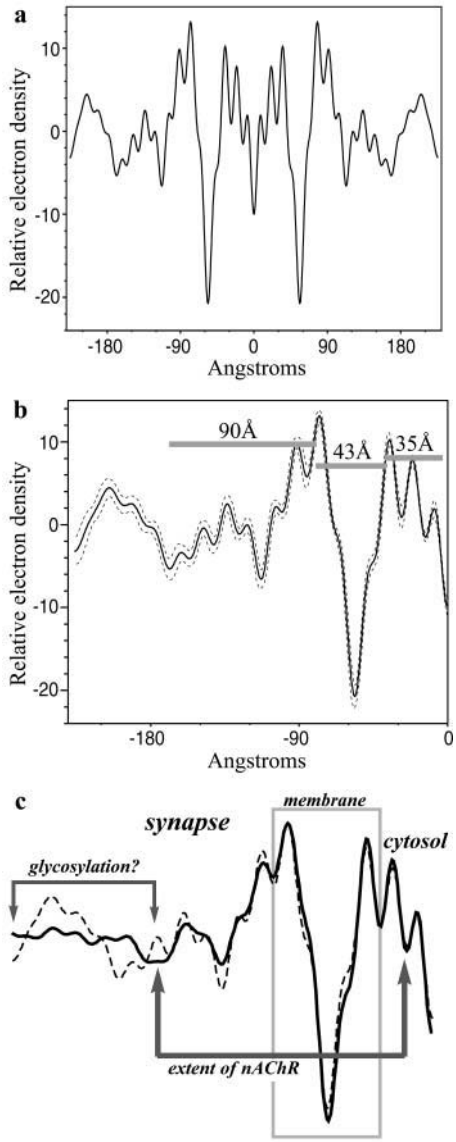

FIGURE 4 (*a*) Average experimental electron density profile structure derived for fully oriented *Torpedo californica* nAChR membranes at 14 Å resolution. Note that the two minima at ±56.5 Å correspond to the methyl troughs of lipid bilayer structures. (*b*) One half of the double-membrane unit cell is shown for clarity from −226 Å to 0 Å. A point-by-point standard deviation of the population ($n = 21$) is shown as an envelope of uncertainty around the mean (*dashed lines*). (*c*) Interpretation of the profile structure. Shown are the average experimental electron density profile structure (*dashed line*) and a profile structure derived from direct application of the phases to the structure factor amplitudes without Gaussian fitting (*solid line*). The membrane bilayer and the synaptic and cytoplasmic sides of the membrane are indicated. The full extent of the nAChR is shown as well as a region postulated to correspond to glycosylation and aqueous space between multilayers.

such variables as hydration state, multilayer sample preparation technique, and multiple nAChR membrane preparations, in an attempt to obtain a truly ''average'' structure. The profile structure presented in Fig. 4 is the average structure obtained for 21 multilayer samples prepared from 10 membrane preparations.

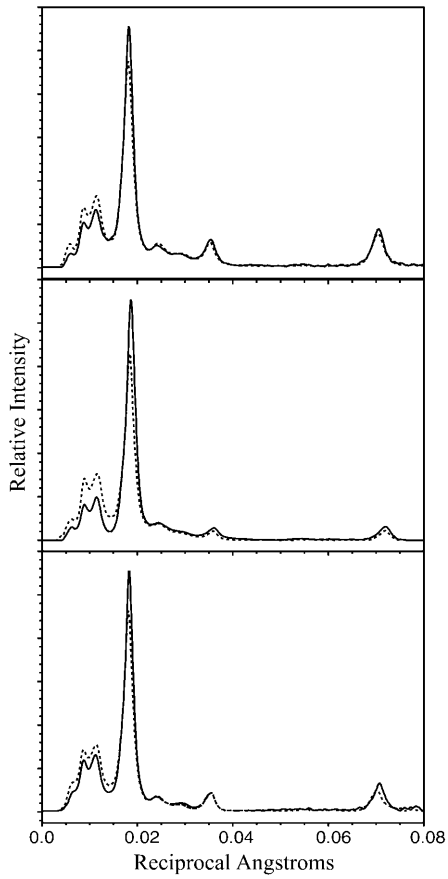

FIGURE 5 The experimental intensity functions, $I_{exp}(s)$s, determined for *Torpedo* nAChR membranes in the absence and presence of α-toxin, corresponding to six matched sample pairs from three membrane preparations. The intensity data are plotted as relative intensity (arbitrary units) versus reciprocal Angstroms (in units of s, where $s = 2\sin(\theta)/\lambda$). Each of the three panels is derived from a separate membrane preparation. Each panel is the average $I_{exp}(s)$ for two matched sample pairs, two samples in the absence (*solid line*) and two samples in the presence (*dashed line*) of α-toxin. These $I_{exp}(s)$s differ by $|\Delta I(s)|/I(s) = 22\%$ (*top panel*), 50% (*middle panel*), and 30% (*bottom panel*).

Within a single membrane preparation and under identical multilayer preparation conditions, the error in $I_{exp}(s)$ was greatly reduced. This error was significantly reduced if all samples originated from the same membrane preparation, and all samples were prepared and handled under identical conditions. With these constraints, error in $I_{exp}(s)$ was reduced to 12%. This error level was tolerable in terms of the observed differences in the lamellar diffraction data for samples prepared in the presence of α-toxin. The average difference in total intensity in the presence of toxin was 34 ± 13%. Moreover, the nAChR membrane multilayer samples were not perturbed by the presence of bound α–toxin. The average lamellar lattice spacings in the absence and presence of α-toxin were 452 Å ± 4 Å ($n = 6$) and 454 Å ± 4 Å ($n = 6$), respectively.

For samples prepared in the absence and presence of α-toxin, the structure factor amplitudes were determined as

described above. It should be noted that for each experimental data set with and without α-toxin, the total corrected and integrated intensity was scaled to a constant value in order to compare data sets between samples (Moody, 1963; Blaurock, 1971). In the presence of α-toxin, there were no changes in the positions of the observed reflections or in the background intensity levels between reflections. The only apparent changes in $I_{exp}(s)$ were in the magnitudes of the observed reflections (Fig. 5).

The structure factor amplitudes were independently phased using the methods described above. Electron density profiles, $\rho(z)s$, in the absence and presence of α-toxin were calculated using each potential phase set. Since the overall form of $I_{exp}(s)$ did not change, it was reasoned that the phases must be the same in the absence and presence of α-toxin. The pattern recognition approach (Luzzati et al., 1972) was used to evaluate difference electron density profiles, $\Delta\rho(z)$, for every unique phase combination. The selection process relied on visual inspection of the $\Delta\rho(z)s$ for the following properties: 1), The differences in the profile structure must be localized; 2), The differences must occur primarily on one side of the membrane bilayer; and 3), There should be a positive difference attributable to the location of the α-toxin molecules (locally, the specific binding of two α-toxin molecules should contribute ~21% more protein mass). Only a single phase set satisfied the above criteria. Moreover, this phase set was arrived at independently and was the same as that described above.

The structure factor amplitudes and phases were used to calculate electron density profiles for each of the six matched sample pairs. After scaling the intensity functions with and without α-toxin to the same constant value (arbitrary units), no scaling or normalization was applied to the electron density profiles. One-half of the double-membrane unit cell is shown in Fig. 6 *a* with the average $\Delta\rho(z)$ calculated from the six sample pairs. A point-by-point standard deviation of the population of $\Delta\rho(z)s$ was calculated and is shown as an envelope of uncertainty around the mean. A positive difference in electron density was observed at ±96 Å (directly apposed to the phospholipid headgroup peak of the lipid bilayer) with a FWHM of ~34 Å (toxin site in Fig. 6 *b*). A second positive difference in electron density was observed at the edges of the unit cell, at ±215 Å with a FWHM of 21 Å. Regions of decreased electron density were observed at ±57 Å and ±141 Å.

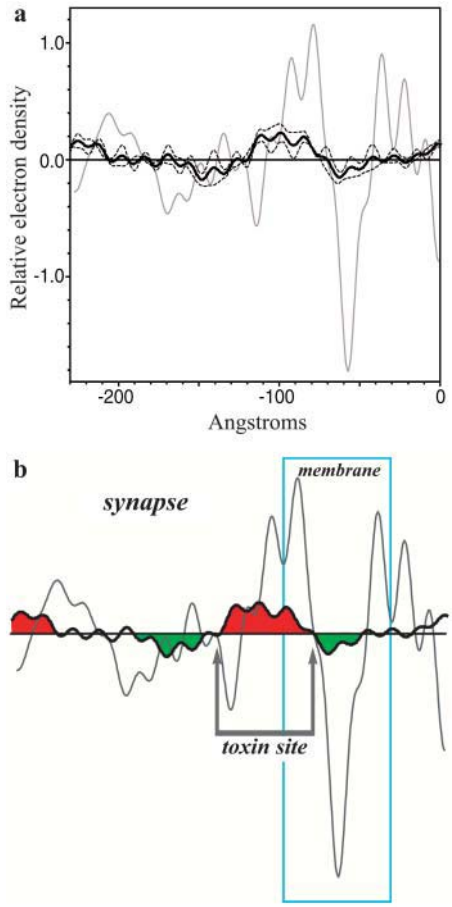

FIGURE 6 (*a*) The electron density profile structure for the nAChR membrane in the absence of toxin (*gray line*) is shown for one-half of the double membrane unit cell from −226 Å to 0 Å. Superimposed is the average difference electron density profile, $\Delta\rho(z)$, calculated from the six matched sample pairs (*black line*). The average $\Delta\rho(z)$ is surrounded by an envelope of uncertainty calculated as a point-by-point standard deviation (*dashed lines*) for the six matched sample pairs. (*b*) Interpretation of the $\Delta\rho(z)$. The membrane bilayer and the synaptic side of the membrane are indicated. Electron density postulated to be the α-toxin binding sites (*red*), additional electron density at the edge of the unit cell (*red*), and regions of decreased electron density (*green*) are shown.

Model calculation

An atomic model for part of the electron density profile structure was calculated using the atomic structures for AChBP (Brejc et al., 2001) and α-toxin (Moise et al., 2002). A complex of AChBP and two α-toxin molecules was constructed and the number of electrons were projected onto the *z* axis parallel with the AChBP channel (Chester et al., 1992). The resultant electron density profiles are shown in Fig. 7 *b*. The number of electrons added locally by the presence of two α-toxin molecules yielded a 21% increase in electron density (calculated between 24 and 58 Å in Fig. 7 *b*; 14% increase overall in the model). The model strongly supports the observed increase in electron density and the interpretation in Fig. 6 *b*.

DISCUSSION

There have been several low angle x-ray diffraction studies of native nAChR membranes (Dupont et al., 1974; Ross et al., 1977; Kistler et al., 1982; Fairclough et al., 1983, 1986). In light of these studies, our goal was to resolve some of the ambiguities concerning the nAChR electron density profile by obtaining high quality, reproducible, moderate

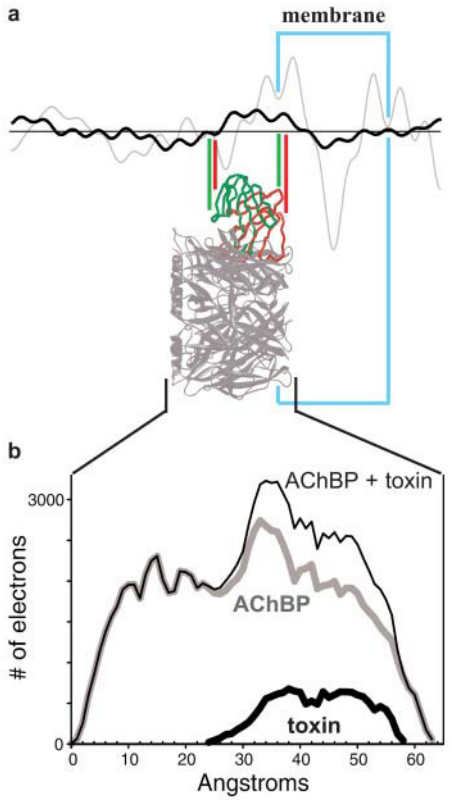

FIGURE 7 (*a*) Comparison of the average difference electron density profile $\Delta\rho(z)$ (*black line*) and the profile structure for the nAChR membrane in the absence of toxin (*gray line*) with the 3D models of Harel et al. (2001) and Moise et al. (2002). In these two models, the AChBP is in gray and α-toxin is in green (Harel et al, 2001) and red (Moise et al., 2002). (*b*) A complex of AChBP (Brejc et al., 2000) and two toxin molecules (Moise et al., 2002) was constructed and the number of electrons was projected onto the *z* axis parallel with the channel for AChBP alone (*thick gray line*), two α-toxin molecules alone (*thick black line*), and the complex of AChBP and two α-toxin molecules (*thin black line*). The resultant electron density profiles are atomic resolution models of the nAChR synaptic domain in the absence and presence of two α-toxin molecules.

resolution, low angle x-ray diffraction data. In addition, this system would allow us to resolve some of the ambiguities concerning the α-toxin binding sites and their proximity to the membrane surface.

Given that the information content in a low angle x-ray scattering profile is low, the question remains exactly how much information is there. A fundamental component of all natural membranes is the fluid state lipid bilayer. Low angle x-ray diffraction has played a central role in understanding bilayer structure, where the ''structure'' of a membrane consists of the average spatial distribution of the lipids and proteins projected onto a line normal to the membrane plane. The electron density difference between the phospholipid headgroups and terminal methyl groups of lipid moieties in a bilayer structure provides the highest contrast elements in our diffraction experiments (Franks and Levine, 1981). In fact, analysis of membrane diffraction data can yield a high degree of spatial resolution and precise localization for both the lipids and proteins comprising a membrane bilayer (Wiener and White, 1991, 1992). As such, this technique was well suited for localizing the α-toxin binding sites relative to the membrane lipid bilayer.

In these studies, we offer an interpretation of the electron density profile that is consistent with our current understanding of the nAChR structure (Fig. 4 *c*). The cytoplasmic domain of the nAChR and rapsyn extend 35 Å from the membrane bilayer surface. The lipid bilayer is asymmetric with a thickness of 43 Å (phospholipid headgroup-to-headgroup distance). The synaptic region of the profile structure is divided into two regions, the nAChR synaptic domain which appears to extend ~90 Å above the bilayer surface and a region we interpret to correspond to the ~20 kDa of nAChR-attached glycosylation (Nomoto et al., 1986; Poulter et al., 1989). This interpretation is in overall agreement with electron cryomicroscopy studies (Toyoshima and Unwin, 1988, 1990; Unwin, 1993, 1995; Miyazawa et al., 1999).

In the multilayer sample preparation employed herein, the nAChR membranes were incubated in the presence of excess α-toxin to maximize binding and complex formation. Important to the diffraction sample preparation procedure are several aspects of the association between α-toxin and nAChR. The long α-toxins have an association rate much slower than the diffusion limit, with 1 min to 1 h required for maximum binding (Klett et al., 1973; Weber and Changeux, 1974; Maelicke et al., 1977; Blanchard et al., 1979). The off-rate of the α-toxins is extremely slow (several hours to many days) and is independent of temperature (Weber and Changeux, 1974; Chicheportiche et al., 1975). Thus, the nAChR multilayer samples prepared in the presence of α-toxin were expected to remain stable during the time course of our experiments. Indeed, differences were readily apparent in the lamellar diffraction data from samples incubated in the presence of α-toxin (Fig. 5).

In the presence of α-toxin, we offer an interpretation of the difference electron density profile consistent with our current understanding of the nAChR structure (Fig. 6 *b*). The $\Delta\rho(z)$ indicated three primary features which were interpreted in the following way. The principle difference was an increase in electron density on the synaptic side of the nAChR membrane, directly apposed to and in apparent contact with the bilayer surface. This increase in electron density measured 34 Å across, in accord with the approximate 40 Å × 30 Å × 20 Å dimensions of α-toxin (Love and Stroud, 1986; Harel et al., 2001; Scarselli et al., 2002; Moise et al., 2002). Thus, the increase in electron density was interpreted as nAChR-bound α-toxin, with the two α-toxin molecules occupying equivalent positions on the α-subunits. Regions of decreased electron density were observed in the $\Delta\rho(z)$ flanking the α-toxin binding sites. These regions of decreased electron density may reflect a conformational change in the nAChR accompanying α-toxin binding (McCarthy and Stroud, 1989; Unwin, 1995). The conformational changes were local to the α-toxin binding sites and encompassed the synaptic and

transmembrane domains of the nAChR. The final change in electron density observed in the $\Delta\rho(z)$ was a small increase in electron density at the edges of the unit cell. This was interpreted as unbound α-toxin trapped between nAChR membrane vesicles during the multilayer sample preparation. More importantly, this increase in electron density was too far from the bilayer surface to correspond to nAChR-bound α-toxin (137 Å above the bilayer surface).

The location of the α-toxin binding sites on the nAChR have been examined using the techniques of low angle x-ray diffraction (Kistler et al., 1982; Fairclough et al., 1983), electron microscopy (Holtzman et al., 1982; Zingsheim et al., 1982; Bon et al., 1984; Kubalek et al., 1987), and fluorescence resonance energy transfer experiments (Herz et al., 1989; Johnson et al., 1990; Valenzuela et al., 1994). In general, low angle x-ray diffraction and electron microscopy experiments have suggested a location for the α-toxin binding sites on the apex of the nAChR synaptic domain. This evidence notwithstanding, more recent electron cryomicroscopy (Unwin, 1993, 1995; Miyazawa et al., 1999) and fluorescence resonance energy transfer (Herz et al., 1989; Johnson et al., 1990; Valenzuela et al., 1994) experiments have suggested a location significantly below the extracellular apex and closer to the membrane surface. This assertion is likely to be correct given the structures of the AChBP (Brejc et al., 2001) and numerous α-toxin complexes (Basus et al., 1993; Zeng et al., 2001; Scherf et al., 1997; Harel et al., 2001; Moise et al., 2002).

CONCLUSION: A MODEL FOR α-TOXIN BINDING

Electron density profiles of one-dimensional arrays, derived by the technique of low angle x-ray diffraction, provide a powerful method for localizing the proteins and lipids that make up native membranes. In our application of this technique, the most striking observation is the proximity of the α-toxin binding sites to the membrane surface. Our profile structures indicate that the bound α-toxins contact the phospholipid headgroups of the lipid bilayer. In other words, the average distribution of the toxin binding sites partially overlaps the average distribution of the phospholipid headgroups of the lipid bilayer. Thus, α-toxin binding may displace lipid headgroups associated with the nAChR, partially explaining the slow on-rate of the long α-toxins (Klett et al., 1973; Weber and Changeux, 1974; Maelicke et al., 1977; Blanchard et al., 1979). Nonetheless, our data confirms and extends a growing body of evidence that α-toxin binds to the side of the nAChR synaptic vestibule. In Fig. 7, two current models of α-toxin binding (Harel et al., 2001; Moise et al., 2002) are compared to the profile structures derived in our studies. While these models rely on the structure of the AChBP (Brejc et al., 2001), our observations apply to the nAChR in its natural environment, the fully hydrated postsynaptic membrane.

The authors thank Drs. Rondi A. Butler, David W. Chester, David G. Rhodes, and Mark W. Trumbore for helpful discussions.

H.S.Y. is supported by a New Investigator, Operating, and Equipment grant from the Canadian Institutes of Health Research (94826) and a Scholar and Establishment grant from the Alberta Heritage Foundation for Medical Research (200100476).

REFERENCES

Agard, D., and R. Stroud. 1982. alpha-Bungarotoxin structure revealed by a rapid method for averaging electron density on noncrystallographically translationally related molecules. *Acta Cryst. Sect. A.* A38:186–194.

Basus, V., G. Song, and E. Hawrot. 1993. NMR solution structure of an alpha-bungarotoxin/nicotinic receptor peptide complex. *Biochemistry.* 32:12290–12298.

Betzel, C., G. Lange, G. Pal, K. Wilson, A. Maelicke, and W. Saenger. 1991. The refined crystal structure of alpha-cobratoxin from Naja naja siamensis at 2.4 Å resolution. *J. Biol. Chem.* 266:21530–21536.

Blanchard, S., U. Quast, K. Reed, T. Lee, M. Schimerlik, R. Vandlen, T. Claudio, C. Strader, H.-P. Moore, and M. Raftery. 1979. Interaction of [^{125}I]-alpha-bungarotoxin with acetylcholine receptor from Torpedo californica. *Biochemistry.* 18:1875–1883.

Blaurock, A. 1971. Structure of the nerve myelin membrane: Proof of the low-resolution profile. *J. Mol. Biol.* 56:35–52.

Blaurock, A. 1975. Bacteriorhodopsin: A trans-membrane pump containing alpha-helix. *J. Mol. Biol.* 93:139–158.

Blaurock, A. 1982. Evidence of bilayer structure and of membrane interactions from x-ray diffraction analysis. *Biochim. Biophys. Acta.* 650:167–207.

Blaurock, A., and M. Wilkins. 1969. Structure of frog photoreceptor membranes. *Nature.* 223:906–909.

Bon, F., E. Lebrun, J. Gomel, R. Van Rappenbusch, J. Cartaud, J.-L. Popot, and J.-P. Changeux. 1984. Image analysis of the heavy form of the acetylcholine receptor from Torpedo marmorata. *J. Mol. Biol.* 176: 205–237.

Brejc, K., W. van Dijk, R. Klaassen, M. Shuurmans, J. van Der Oost, A. Smit, and T. Sixma. 2001. Crystal structure of an ACh-binding protein reveals the ligand-binding domain of nicotinic receptors. *Nature.* 411:269–276.

Chester, D., L. Herbette, R. Mason, A. Joslyn, D. Triggle, and D. Koppel. 1987. Diffusion of dihydropyridine calcium channel antagonists in cardiac sarcolemmal lipid multibilayers. *Biophys. J.* 52:1021–1030.

Chester, D. W., V. Skita, H. S. Young, T. Mavromoustakos, and P. Strittmatter. 1992. Bilayer structure and physical dynamics of the cytochrome b5 dimyristoylphosphatidylcholine interaction. *Biophys. J.* 61:1224–1243.

Chiapinelli, V. 1993. *In* Natural and Synthetic Neurotoxins. A. Harvey, editor. Academic Press, New York. 65–128.

Chicheportiche, R., J. Vincent, C. Kopeyan, H. Schweitz, and M. Lazdunski. 1975. Structure-function relationships in the binding of snake neurotoxins to the Torpedo membrane receptor. *Biochemistry.* 14:2081–2091.

Dupont, Y., J. B. Cohen, and J.-P. Changeux. 1974. X-ray diffraction study of membrane fragments rich in acetylcholine receptor protein prepared from the electric organ of Torpedo marmarota. *FEBS Lett.* 40:130–133.

Fairclough, R., J. Finer-Moore, R. Love, D. Kristofferson, P. Desmueles, and R. Stroud. 1983. Subunit organization and structure of an acetylcholine receptor. *Cold Spring Harb. Symp. Quant. Biol.* 48:9–20.

Fairclough, R., R. Maike-Lye, R. Stroud, K. Hodgson, and S. Doniach. 1986. Location of terbium binding sites on acetylcholine receptor-enriched membranes. *J. Mol. Biol.* 189:673–680.

Franks, N., and Y. Levine. 1981. Low angle x-ray diffraction. *In* Membrane Spectroscopy. E. Grell, Editor. Springer-Verlag, New York, NY.

Gruner, S., D. Barry, and G. Reynolds. 1982. X-ray diffraction analysis of wet isolated bovine rod outer segment disks. A dehydration study. *Biochim. Biophys. Acta*. 690:187–198.

Harel, M., R. Kasher, A. Nicolas, J. Guss, M. Balass, M. Fridkin, A. Smit, K. Brejc, T. Sixma, E. Katchalski-Katzir, J. Sussman, and S. Fuchs. 2001. The binding site of acetylcholine receptor as visualized in the x-ray structure of a complex between alpha-bungarotoxin and a mimotope peptide. *Neuron*. 32:265–275.

Herbette, L., J. Marquadt, A. Scarpa, and J. Blasie. 1977. A direct analysis of lamellar x-ray diffraction from hydrated oriented multilayers of fully functional sarcoplasmic reticulum. *Biophys. J*. 20:245–272.

Herz, J., D. Johnson, and P. Taylor. 1989. Distance between the agonist and noncompetitive inhibitor sites on the nicotinic acetylcholine receptor. *J. Biol. Chem*. 264:12439–12448.

Holtzman, E., D. Wise, J. Wall, and A. Karlin. 1982. Electron microscopy of complexes of isolated acetylcholine receptor, biotinyl-toxin, and avidin. *Proc. Natl. Acad. Sci. USA*. 79:310–314.

Hosemann, R., and S. Bagchi. 1962. Direct Analysis of Diffraction by Matter. North-Holland, Amsterdam.

Johnson, D., R. Cushman, and R. Malekzadeh. 1990. Orientation of cobra alpha-toxin on the nicotinic acetylcholine receptor. Fluorescence studies. *J. Biol. Chem*. 265:7360–7368.

Kistler, J., and R. Stroud. 1981. Crystalline arrays of membrane-bound acetylcholine receptor. *Proc. Natl. Acad. Sci. USA*. 78:3678–3682.

Kistler, J., R. Stroud, M. Klymkowsky, R. Lalancette, and R. Fairclough. 1982. Structure and function of an acetylcholine receptor. *Biophys. J*. 37:371–383.

Klett, R., B. Fulpius, D. Cooper, M. Smith, E. Reich, and L. Possani. 1973. The acetylcholine receptor. I. Purification and characterization of a macromolecule isolated from Electrophorus electricus. *J. Biol. Chem*. 248:6841–6853.

Klymkowsky, M., J. Heuser, and R. Stroud. 1980. Protease effects on the structure of acetylcholine receptor membranes from Torpedo californica. *J. Cell Biol*. 85:823–838.

Kubalek, E., S. Ralston, L. Lindstrom, and N. Unwin. 1987. Location of subunits within the acetylcholine receptor by electron image analysis of tubular crystals from Torpedo marmorata. *J. Cell Biol*. 105:9–18.

Laemmli, U. 1970. Cleavage of structural proteins during the assembly of the head of bacteriophage T4. *Nature*. 227:680–685.

LaRochelle, W., and S. Froehner. 1986. Determination of the tissue distributions and relative concentrations of the postsynaptic 43kDa protein and the acetylcholine receptor in Torpedo. *J. Biol. Chem*. 261:5270–5274.

Leroy, E., A. Mikou, Y. Yang, and E. Guittet. 1994. The three-dimensional NMR structure of alpha-cobratoxin at pH 7.5 and conformational differences with the NMR solution structure at pH 3.2. *J. Biomol. Struct. Dyn*. 12:1–17.

Lesslauer, W. 1978. Phytohemagglutinin and transmembrane proteins in agglutinated sheep erythrocyte ghost membranes. *Biochim. Biophys. Acta*. 510:264–269.

Love, R., and R. Stroud. 1986. The crystal structure of alpha-bungarotoxin at 2.5Å resolution: Relation to solution structure and binding to acetylcholine receptor. *Protein Eng*. 1:37–46.

Lukas, R., H. Morimoto, M. Hanley, and E. Bennett. 1981. Radiolabeled alpha-bungarotoxin derivatives: Kinetic interaction with nicotinic acetylcholine receptors. *Biochemistry*. 20:7373–7378.

Luzzati, V., A. Tardieu, and D. Taupin. 1972. A pattern recognition approach to the phase problem: Application to the x-ray diffraction study of biological membranes and model systems. *J. Mol. Biol*. 64:269–286.

Maelicke, A., B. Fulpius, R. Klett, and E. Reich. 1977. Acetylcholine receptor: Responses to drug binding. *J. Biol. Chem*. 252:4811–4830.

Makowski, L., D. Caspar, W. Phillips, and D. Goodenough. 1977. Gap junction structures II: Analysis of the x-ray diffraction data. *J. Cell Biol*. 74:629–645.

McCarthy, M. P., and R. M. Stroud. 1989. Conformational states of the nicotinic acetylcholine receptor from *Torpedo californica* induced by the binding of agonists, antagonists and local anesthetics. Equilibrium measurement using tritium-hydrogen exchange. *Biochemistry*. 28:40–48.

Miyazawa, A., Y. Fujiyoshi, M. Stowell, and N. Unwin. 1999. Nicotinic acetylcholine receptor at 4.6 Å resolution: transverse tunnels in the channel wall. *J. Mol. Biol*. 288:765–786.

Moise, L., A. Piserchio, V. Basus, and E. Hawrot. 2002. NMR structural analysis of alpha-bungarotoxin and its complex with the principal alpha-neurotoxin-binding sequence on the alpha 7 subunit of a neuronal nicotinic acetylcholine receptor. *J. Biol. Chem*. 277:12406–12417.

Moody, M. 1963. X-ray diffraction pattern of nerve myelin: A method for determining the phases. *Science*. 142:1173–1174.

Mulac-Jericevic, B., and M. Z. Atassi. 1986. Segment alpha 182–198 of *Torpedo californica* acetylcholine receptor contains a second toxin-binding region and binds anti-receptor antibodies. *FEBS Lett*. 199:68–74.

Neumann, D., D. Barchan, M. Fridkin, and S. Fuchs. 1986b. Analysis of ligand binding to the synthetic dodecapeptide 185–196 of the acetylcholine receptor alpha subunit. *Proc. Natl. Acad. Sci. USA*. 83:9250–9253.

Neumann, D., D. Barchan, A. Safran, J. M. Gershoni, and S. Fuchs. 1986a. Mapping of the a-bungarotoxin binding site within the alpha subunit of the acetylcholine receptor. *Proc. Natl. Acad. Sci. USA*. 83:3008–3001.

Nomoto, H., N. Takahashi, Y. Nagaki, S. Endo, Y. Arata, and K. Hayashi. 1986. Carbohydrate structures of acetylcholine receptor from *Torpedo californica* and distribution of oligosaccharides among the subunits. *Eur. J. Biochem*. 157:233–242.

Pachence, J., R. Fischetti, and J. Blasie. 1989. Location of the heme-Fe atoms within the profile structure of a monolayer of cytochrome c bound to the surface of an ultrathin lipid multilayer film. *Biophys. J*. 56:327–337.

Phillips, W., and G. Phillips. 1985. Two new x-ray films: Conditions for optimum development and calibration of response. *J. Appl. Crystallogr*. 18:3–7.

Poulter, L., J. P. Earnest, R. M. Stroud, and A. L. Burlingame. 1989. Structure, oligosaccharide structures, and posttranslationally modified sites of the nicotinic acetylcholine receptor. *Proc. Natl. Acad. Sci. USA*. 86:6645–6649.

Raftery, M., M. Hunkapillar, C. Strader, and L. Hood. 1980. Acetylcholine receptor: Complex of homologous subunits. *Science*. 208:1454–1456.

Ralston, S., V. Sarin, H. L. Thanh, J. Rivier, J. L. Fox, and J. Lindstrom. 1987. Synthetic peptides used to locate the alpha-bungarotoxin binding site and immunogenic regions on alpha subunits of the nicotinic acetylcholine receptor. *Biochemistry*. 26:3261–3266.

Ross, M., M. Klymkowsky, D. Agard, and R. Stroud. 1977. Structural studies of a membrane-bound acetylcholine receptor from Torpedo californica. *J. Mol. Biol*. 116:635–659.

Scarselli, M., O. Spiga, A. Ciutti, A. Bernini, L. Bracci, B. Lelli, L. Lozzi, D. Calamandrei, D. Di Maro, S. Klein, and N. Niccolai. 2002. NMR structure of alpha-bungarotoxin free and bound to a miotope of the nicotinic acetylcholine receptor. *Biochemistry*. 41:1457–1463.

Scherf, T., M. Balass, S. Fuchs, E. Katchalski-Katzir, and J. Anglister. 1997. Three-dimensional solution structure of the complex of alpha bungarotoxin with a library-derived peptide. *Proc. Natl. Acad. Sci. USA*. 98:6059–6064.

Schmidt, J., and M. A. Raftery. 1973. A simple assay for the study of solubilized acetylcholine receptor. *Anal. Biochem*. 52:349–354.

Schwartz, S., J. Cain, E. Dratz, and J. Blasie. 1975. An analysis of lamellar x-ray diffraction from disordered membrane multilayers with application to data from retinal rod outer segments. *Biophys. J*. 15:1201–1233.

Servent, D., V. Winckler-Dietrich, H. Hu, P. Kessler, P. Drevet, D. Bertrand, and A. Menez. 1997. Only snake curaremimetic toxins with a fifth disulfide bond have high affinity for the neuronal alpha7 nicotinic receptor. *J. Biol. Chem*. 272:24279–24286.

Toyoshima, C., and P. Unwin. 1988. Ion channel of the acetylcholine receptor reconstructed from images of postsynaptic membranes. *Nature*. 336:247–250.

Toyoshima, C., and P. Unwin. 1990. Three-dimensional structure of the acetylcholine receptor by cryo-electron microscopy and helical image reconstruction. *J. Cell Biol.* 111:2623–2635.

Unwin, N. 1993. Nicotinic acetylcholine receptor at 9 Å resolution. *J. Mol. Biol.* 229:1101–1124.

Unwin, N. 1995. Acetylcholine receptor channel imaged in the open state. *Nature.* 373:37–43.

Unwin, N., A. Miyazawa, J. Li, and Y. Fujiyoshi. 2002. Activation of the nicotinic acetylcholine receptor involves a switch in conformation of the alpha subunits. *J. Mol. Biol.* 319:1165–1176.

Valenzuela, C. F., P. Weign, J. Yguerabide, and D. A. Johnson. 1994. Transverse distance between the membrane and the agonist binding sites on the Torpedo acetylcholine receptor: A fluorescence study. *Biophys. J.* 66:674–682.

Weber, M., and J.-P. Changeux. 1974. Binding of *Naja nigricollis* [^{3}H] alpha-toxin to membrane fragments from Electrophorus and Torpedo electric organs. I. Binding of the tritiated alpha-neurotoxin in the absence of effector. *Mol. Pharmacol.* 10:1–14.

Wiener, M., and S. White. 1991. Fluid bilayer structure determination by the combined use of x-ray and neutron diffraction. I. Fluid bilayer models and the limits of resolution. *Biophys. J.* 59:162–173.

Wiener, M., and S. White. 1992. Structure of a fluid dioleoylphosphatidylcholine bilayer determined by joint refinement of x-ray and neutron diffraction data. III. Complete structure. *Biophys. J.* 61:437–447.

Wilson, P. T., and T. L. Lentz. 1988. Binding of alpha-bungarotoxin to synthetic peptides corresponding to residues 173–204 of the subunit of Torpedo, calf and human acetylcholine receptor and restoration of high affinity binding by sodium dodecyl sulfate. *Biochemistry.* 27: 6667–6674.

Wilson, P. T., T. L. Lentz, and E. Hawrot. 1985. Determination of the primary amino acid sequence specifying the alpha-bungarotoxin binding site on the alpha subunit of the acetylcholine receptor from *Torpedo californica*. *Proc. Natl. Acad. Sci. USA.* 82:8790–8794.

Young, H. S., V. Skita, R. P. Mason, and L. G. Herbette. 1992. Molecular basis for the inhibition of 1,4-dihydropyridine calcium channel drugs binding to their receptors by a nonspecific site interaction mechanism. *Biophys. J.* 61:1244–1255.

Zeng, H., L. Moise, M. Grant, and E. Hawrot. 2001. The solution structure of the complex formed between alpha-bungarotoxin and an 18-mer cognate peptide derived from the alpha 1 subunit of the nicotinic acetylcholine receptor from Torpedo californica. *J. Biol. Chem.* 276: 22930–22940.

Zingsheim, H. P., F. J. Barrantes, J. Frank, W. Hanicke, and D.-C. Neugebauer. 1982. Direct structural localization of two toxin-recognition sites on an ACh receptor protein. *Nature.* 299:81–84.

Zinn-Justin, S., C. Roumestand, B. Gilquin, F. Bontems, A. Menez, and F. Toma. 1992. Three-dimensional solution structure of a curaremimetic toxin from Naja nigricolis venom: a proton NMR and molecular modeling study. *Biochemistry.* 31:11335–11347.